CDK1 controls CHMP7-dependent nuclear envelope reformation

Alberto T Gatta[1,2,†], Yolanda Olmos[1,2,3,†], Caroline L Stoten[1,2,†] and Jeremy G Carlton[1,2,*]

1. School of Cancer and Pharmaceutical Sciences, King's College London, SE1 1UL, UK
2. The Francis Crick Institute, 1 Midland Road, London, NW1 1AT, UK
3. Current Address: Department of Cell Biology, Universidad Complutense de Madrid, Madrid, Spain

* Correspondence to: jeremy.carlton@kcl.ac.uk

† These authors contributed equally to the study

Abstract

Through the process of annular fusion and disassembly of spindle microtubules, the Endosomal Sorting Complex Required for Transport-III (ESCRT-III) machinery has emerged as a key player in the regeneration of a sealed nuclear envelope during mitotic exit, and in the repair of this organelle during interphase rupture. ESCRT-III polymerisation at the nuclear envelope occurs transiently during mitotic exit and CHMP7, an ER-localised ESCRT-II/ESCRT-III hybrid protein, initiates assembly in a manner dependent upon the INM protein LEM2. Whilst classical nucleocytoplasmic transport mechanisms have been proposed to separate LEM2 and CHMP7 during interphase, it is unclear how CHMP7 assembly is suppressed in mitosis when NE and ER identities are mixed. Here, we use live cell imaging and protein biochemistry to examine the biology of these proteins during mitotic exit. We show that CHMP7 plays an important role in disaggregating LEM2 clusters at the reforming nuclear envelope during mitotic exit to allow proper nuclear regeneration. Further, we show that CDK1 phosphorylates CHMP7 upon mitotic entry and suppresses its polymerisation, preventing its inappropriate capture of LEM2 in the peripheral ER during mitotic exit. Lastly, we establish that a microtubule network is dispensable for ESCRT-III assembly at the reforming nuclear envelope. These data identify a key cell-cycle control programme allowing ESCRT-III-dependent nuclear regeneration.

Main Text

As cells exit division they must regenerate both their nuclei and their nuclear envelope. ER membranes enveloping nascent daughter nuclei must be sealed through the process of annular fusion, and inner nuclear membrane proteins must be properly inserted to tether the nuclear envelope to the nuclear lamina and chromatin masses. ESCRT-III is a key orchestrator of nuclear envelope sealing during open mitosis [1-4], the repair of ruptured micro- and parental nuclear envelopes in interphase [5-10] and the surveillance of damaged NPC complexes in *S. cerevisiae* [11,12]. The inner nuclear membrane protein LEM2 assembles into a phase-separated gel-like polymer that is thought to define sites of ESCRT-dependent annular fusion through its ability to recruit and activate polymerisation of the ESCRT-III protein, CHMP7 [4,6]. Furthermore, CHMP7 and LEM2 may also regulate nuclear envelope sealing by feeding new ER membrane, as recently shown in *C. elegans* [13]. In worms and fission yeast, LEM2 also has important roles in stabilizing peripheral heterochromatin and in organising chromatin architecture in the interphase nucleus [14-16]. We found that in early mitosis, GFP-CHMP7 and LEM2-mCh co-localised in a hybrid ER/NE, were then transiently co-enriched at sites of ESCRT-III assembly at the reforming NE, and subsequently adopted distinct ER and NE identities as cells exited mitosis (Figure 1A, Movie 1). As expected [4], LEM2-depletion prevented the transient assembly of CHMP7 at the reforming NE (Figure 1B, Movie 2). We generated cells stably expressing LEM2-mCh or LEM2$^{\delta LEM}$-mCh (Figure S1A) and found that the LEM-domain was necessary for efficient LEM2 and CHMP7 enrichment at the reforming nuclear envelope, and subsequent retention of LEM2 at the NE (Figure S1B and Movie 3). In cells co-expressing GFP-CHMP7 and LEM2$^{\delta LEM}$-mCh, both proteins instead co-polymerised in the peripheral ER after nuclear envelope reformation (Figure S1C). Deletion of the CHMP7-interaction domain from LEM2 (LEM2$^{\delta 415\text{-}485}$-mCh, [6]) also resulted in the generation of clusters of LEM2 and nuclear envelope morphology defects in the following interphase (Figure S1D). These data suggest that LEM2 must effectively gain chromatin tethers during mitotic exit to localise CHMP7 polymerisation to the reforming NE, and that persistent LEM2 in the peripheral ER can seed inappropriate CHMP7 polymerisation during mitotic exit. In *S. japonicus*, Cmp7 plays a role in disaggregating Lem2 clusters during interphase and mitotic exit [16,17]. In mammalian cells, we found that CHMP7 depletion led to persistent enrichment of LEM2 at the reforming NE (Figure 1C, Figure 1D and Movie 4), suggesting that CHMP7 acts additionally to disassemble LEM2 and promote its mobility within the INM. Importantly, depletion of IST1, an ESCRT-III subunit with well-characterised roles in nuclear envelope sealing [2], did not lead to persistent LEM2 clusters (Figure S1E), which is consistent with recent findings from yeast and worms suggesting functional diversity across ESCRT-III components during NE reassembly [13,16]. Persistent assembly of LEM2 in CHMP7-depleted cells led to the formation of NE morphology defects during cytokinesis that persisted into the subsequent interphase (Figure 1E and Figure 1F). These LEM2 clusters did not incorporate other INM proteins such as LAP1 or Emerin (Figure S1F and S1G). Thus, as well as roles in spindle disassembly [2,6] and membrane fusion [2-4], we believe that CHMP7 also controls a separate process of LEM2 disaggregation during mitotic exit. In *S. japonicus*, Lem2 clusters generated in the absence of ESCRT-

III sequester heterochromatin [16]. We wondered if persistent LEM2 aggregation during mitotic exit may perturb chromatin structure in CHMP7-depleted mammalian cells. We followed endogenous Heterochromatin Protein 1 (HP1) after CHMP7 depletion and instead found diminished HP1 foci in these cells (Figure S1H). This defect was more pronounced in cells exhibiting LEM2-mCh clusters (Figure S1I and S1J). From this, we conclude that CHMP7 is necessary for declustering LEM2 during mitotic exit to allow both generation of a normal nuclear envelope and levels of heterochromatin during the following interphase.

We reasoned that spatiotemporal regulation of the LEM2/CHMP7 interaction would be essential both during mitotic exit and in the subsequent interphase. CHMP7 contains predicted Nuclear Export Sequences (NESs) in Helices 5 and 6 that are thought to limit its exposure to INM proteins, including LEM2, during interphase [10,18]. We confirmed the presence of active NESs in helices 5 and 6 of CHMP7 (Figure S2A-S2E) and demonstrated that transient perturbation of exportin function resulted in nuclear accumulation of GFP-CHMP7 (Figure S2D). Transient transfection of NES-compromised CHMP7 constructs led to sequestration of LEM2-mCh in nuclear and cytosolic clusters during interphase, with an additive effect observed upon disrupting both NESs (Figure S2F). The nature of these nuclear clusters remains enigmatic, but consistent with findings that LEM2 forms liquid-like phase separated clusters [6], we observed colocalisation with endogenous promyelocytic leukemia (PML) nuclear bodies (Figure S2G). Despite repeated attempts, we were unable to generate cells constitutively expressing GFP-CHMP7^{2xNES-}. However, by transient transduction of cells with retroviruses driving weak GFP-CHMP7^{2xNES-} expression, we could demonstrate the inappropriate capture of LEM2 during interphase in GFP-CHMP7^{2xNES-}-positive nuclear envelope and cytoplasmic clusters (Figure S2H). These data highlight the essential nature of the trans-nuclear envelope segregation of LEM2 and CHMP7, suggesting the existence of a surveillance system poised to monitor the integrity of this barrier [10,18]. The second NES in Helix6 overlaps with a predicted type-1 MIM ([19], Figure S2A), suggesting that this region may regulate both nucleocytoplasmic compartmentalisation and the ability of CHMP7 to engage the AAA-ATPase, VPS4. While deletion of Helix6 mimicked abrogation of Helix6's NES by elevating nucleoplasmic localisation, it also induced the appearance of CHMP7 clusters at the NE and in the peripheral ER (Figure S2I and S2J). We wondered if this was due to impaired CHMP7 disassembly due to compromised interaction with VPS4. However, we found that CHMP7's C-terminus was unable to bind the isolated VPS4 MIT domain, and careful analysis revealed that charge substitutions at two critical acidic residues has inactivated the predicted type-1 MIM in CHMP7's Helix6 (Figure S2K).

When following cells expressing GFP-CHMP7$^{\delta Helix6}$ through mitotic exit, we were surprised to find that this protein failed to assemble at the NE, but instead polymerised in a timely, but spatially inappropriate manner in the peripheral ER (Figure 2A, Movie 5), sequestering downstream ESCRT-III subunits, such as IST1 (Figure 2B), and LEM2-mCh (Figure 2C) into these clusters. These assemblies persisted into the next interphase, retaining incorporation of ESCRT-III components and LEM2-mCh and preventing LEM2 from

adopting its normal interphase INM localisation (Figure 2D). Given the absence of regulated nucleocytoplasmic transport during this phase of mitosis, and the absence of a functional MIM in CHMP7 (Figure S2K), these data argue against canonical VPS4-binding or the CHMP7-NESs as contributing to this spatially inappropriate polymerisation. Removal of the C-terminal regulatory region of ESCRT-III subunits is thought to convert them into an 'open' conformation, facilitating their polymerisation [20]. We found that GFP-CHMP7$^{\delta Helix6}$ could more efficiently precipitate partner ESCRT-III subunits (Figure 2E, Figure S2L), suggesting that like the described *S. cerevisiae* Chm7^{open} [11], its autoinhibition has been relieved. Turning to a recombinant system, we discovered that polymeric CHMP7 was able to capture and co-precipitate LEM2^{CT}, suggesting how unrestrained CHMP7 polymerisation could lead to sequestration of LEM2 (Figure 2F)

When analysing our time-lapse data, we noticed that interphase assemblies of GFP-CHMP7$^{\delta Helix6}$ were efficiently disassembled upon entry into the next mitosis, but reformed again during mitotic exit (Figure 3A, Figure 3B and Movie 6). Indeed, GFP-CHMP7 and GFP-CHMP7$^{\delta Helix6}$ were indistinguishable during metaphase and anaphase (see anaphases in Figure 1A and Figure 2A). We wondered if there existed a 'reset' mechanism on the polymerisation status of CHMP7 during mitotic entry, to prepare it for spatiotemporally controlled polymerisation during mitotic exit. By capturing GFP-CHMP7 from interphase or mitotic cells, we discovered that CHMP7 was phosphorylated upon mitotic onset (Figure 3C). We mapped sites of mitotic phosphorylation to Ser3 in CHMP7's N-terminus and to Ser441 in CHMP7's C-terminus (Figure 3D, Figure S3A-F). Both sites conform to consensus sequences ([K/H]-[pS]-[P] or [pS]-[P]-[X]-[R/K]) for the major mitotic kinase CDK1 and we could detect modification of these sites in immunoprecipitated samples from M-phase extracts using phospho-specific antibodies directed against these CDK1 substrate phosphorylation sites (Figure 3C).

We next used monopolar spindle assays [21] to examine the synchronised behaviour of CHMP7 during mitotic exit. Here, we synchronised cells at prometaphase using the Eg5 inhibitor STLC [22] and then employed RO-3306, a highly specific CDK1 inhibitor [23], to force mitotic exit. We used previously described CAL-51 cells in which the *CHMP7* locus was homozygously edited to encode mNG-CHMP7 [3]. Following STLC arrest, mNG-CHMP7 initiated assembly 16.32 ± 0.88 minutes after CDK1 inhibition and polymerised in a wave around the chromatin mass from the spindle-distal to the spindle-engaged face (Figure 3E, Figure 3F and Movie 7). Assembly of endogenous CHMP7 persisted for 2.67 ± 0.22 minutes (Figure 3F), mimicking the assembly dynamics around the telophase nuclear envelope in asynchronous cells both in duration and in that CHMP7 in the peripheral ER was resistant to the assembly signal. In CHMP7-depleted HeLa cells stably expressing siRNA-resistant GFP-CHMP7 (GFP-CHMP7^{R}), CHMP7 assembled with similar kinetics, initiating 16.93 ± 1.21 minutes after CDK1 inhibition and persisting for 3.32 ± 0.13 minutes (Figure 3F, Figure S3E and Movie 8). Importantly, LEM2-mCh with similar kinetics, becoming enriched at the monopolar nuclear envelope 16.21 ± 2.23 minutes after CDK1 inhibition, and persisting for 4.11 ± 0.44 minutes. In

contrast to CHMP7, LEM2-mCh localised more strongly at the spindle-engaged face of the NE (Figure 3F, Figure 3G and Movie 9) before being depolymerised and maintaining NE localisation (Figure 3G), which is perhaps indicative of its phase-separated interaction with microtubules [6]. We next asked whether microtubules were necessary for CHMP7 polymerisation by using nocodazole instead of STLC to arrest cells at pro-metaphase. In this case, endogenous mNG-CHMP7 assembled and disassembled at the nuclear envelope with normal kinetics (Figure 3F, Figure S3G, Movie 10), suggesting that microtubules are dispensable for ESCRT-III assembly at this site. Interestingly, endogenous mNG-CHMP7 usually assembled synchronously around the perimeter of the chromatin mass (Figure 3E). However, in the minority of cells that were able to form a pseudo-furrow [21], CHMP7 polymerisation initiated at the furrow-proximal face, before spreading to the rest of the chromatin, suggesting that there may be a furrow-directed spatial component to ESCRT-III assembly at the reforming NE (Figure S3F, Movie 11). Consistent with experiments from cycling cells (Figure 1), in CHMP7-depleted cells stably expressing LEM2-mCh, LEM2-mCh was poorly disassembled after nuclear envelope enrichment (Figure S3H, Figure S3I and Movie 12). These persistent LEM2-mCh assemblies did not colocalise with microtubules, indicating that they do not form as a consequence of impaired spindle disassembly (Figure S3I). Biochemical analysis of whole cell lysates from these monopolar spindle assays revealed phosphorylation of CHMP7 at both S3 and S441 persisted for 20 minutes following CDK1 inhibition, with dephosphorylation completing 30 minutes after CDK1 inhibition (Figure 3H and Figure 3I). Importantly, these data suggest that ESCRT-III-dependent nuclear envelope reformation occurs in a time period when CHMP7 is globally phosphorylated, and that CHMP7 dephosphorylation occurs after nuclear envelope reformation. Although we cannot discount local-dephosphorylation as being a trigger for assembly at the nuclear envelope, inhibition of the major mitotic phosphatases PP1 and PP2A with okadaic acid or calyculin A did not influence assembly dynamics of CHMP7 at the reforming nuclear envelope (Figure S3J).

To examine the role of CDK1-dependent CHMP7 phosphorylation during mitosis, we examined cells stably expressing GFP-CHMP7^{R} S3A, S441A. These cells displayed inappropriate assemblies of CHMP7 and ESCRT-III during interphase (Figure 4A and Figure 4B). Whereas limited polymerisation throughout the peripheral ER was observed during metaphase and early anaphase (Figure 4B and Figure S4A), immediately after NE reformation, these sites of precocious polymerisation grew (Figure 4C, Movie 13). Using a previously described assay that employed sedimentation to report CHMP7 polymerisation [6], we found that recombinant CHMP7 could be directly phosphorylated by CDK1/CCNB1 *in vitro* and that CDK1-phosphorylation suppressed CHMP7 polymerisation (Figure 4D). These data suggest that CDK1 phosphorylation directly suppresses CHMP7 polymerisation which, given the ability of polymeric CHMP7 to capture LEM2 (Figure 2F), may prevent its inappropriate sequestration of LEM2 during mitotic exit. We next generated stable cell lines expressing both LEM2-mCh and GFP-CHMP7^{R} S3A, S441A and imaged them during mitotic exit after CHMP7 depletion. These data revealed that in cells reliant upon GFP-CHMP7^{R} S3A, S441A, whilst LEM2 and CHMP7 enrichment at the reforming INM was unperturbed, LEM2 was additionally incorporated into

precocious extra-nuclear GFP-positive clusters during mitotic exit and failed to adopt its normal distribution at the INM (Figure 4E, Figure S4B and Movie 14). These clusters displayed fusogenic behaviour (Figure S4C and Movie 15) and long-term culture of cells bearing GFP-CHMP7^{R} S3A S441A resulted in the loss of LEM2 from the INM with its retention in singular cytoplasmic clusters (Figure S4D and Movie 15). These data highlight CDK1-phosphorylation of CHMP7 as a mechanism to restrict precocious LEM2 capture during mitotic exit and to ensure that the nucleus reforms with its proper complement of INM proteins for the following interphase.

Discussion

During mitosis, the cell is challenged by the problem of how to suppress ESCRT-III polymerisation when both CHMP7 and its partner protein LEM2 are in the same hybrid ER/NE membrane and regulated nucleocytoplasmic transport mechanisms are inactive. The cell also has to convert an apolar sheet of ER to a polarised sheet with distinct INM and ONM identities. We found that during mitotic exit, the INM protein LEM2 was co-enriched with CHMP7 at the reforming nuclear envelope. Importantly, LEM2 assembly at the reforming nuclear envelope occurred in the absence of CHMP7, suggesting that LEM2 is upstream and does not form part of the ESCRT-III polymer. However, consistent with recent reports from *S. japonicus* [16,17], LEM2's failure to be disassembled in the absence of CHMP7 suggests that CHMP7 acts to decluster and proper release of LEM2, allowing it to correctly populate the INM. Our biochemical data indicate that polymeric CHMP7 can capture LEM2, raising the possibility that this INM protein may instead be a 'cargo' that is actively sorted onto the INM through the activity of CHMP7 at sites of annular fusion. We reasoned that the ability of CHMP7 and LEM2 to interact ought to be tightly regulated during interphase and mitosis. While classical nucleocytoplasmic transport mechanisms act to separate these proteins during interphase [10,18], cells also need to suppress this interaction during mitosis when nuclear envelope and ER membranes are mixed. By inducing precocious polymerisation of CHMP7 through deletion of a C-terminal autoregulatory helix, we were able to show that these clusters were disassembled upon mitotic entry. These data suggested that CHMP7 assembly may be regulated by classical cell cycle control mechanisms and allowed us to identify direct CDK1 phosphorylation of CHMP7 at S3 and S441 as a suppressor of CHMP7 assembly. Interestingly, CHMP7 is the only ESCRT-III subunit to bear recognisable consensus sequences for CDK1 phosphorylation, suggesting that mitotic regulation of ESCRT-III may be effected through this protein. Analysing the kinetics of CHMP7 phosphorylation revealed that phosphorylation persisted during the time of ESCRT-III assembly at the reforming nuclear envelope. Consistent with this, GFP-CHMP7 S3A, S441A still assembled and disassembled at the reforming nuclear envelope and inhibitors of major mitotic exit phosphatases did not alter the kinetics of this process. However, GFP-CHMP7 S3A, S441A displayed additional spatially inappropriate polymerisation and capture of residual LEM2 in the peripheral ER during mitotic exit. While we cannot rule out that the minor pool of CHMP7 in contact with the reforming nucleus is dephosphorylated to trigger assembly before the global pool of CHMP7 in the peripheral ER, these data suggest that phosphorylation acts

as a suppressor of non-specific capture of LEM2 by CHMP7 rather than regulating polymerisation at the reforming nuclear envelope. Indeed, as LEM2 is both necessary for CHMP7 polymerisation [4,6] and can be captured by polymeric CHMP7, these data raise the possibility that LEM2-induced CHMP7 polymerisation may be self-seeding. Finally, contrary to the prevailing view that this assembly occurs at sites where spindle microtubules traverse the reforming nuclear envelope, we found that microtubules are in fact dispensable for CHMP7 assembly at this organelle. These data are consistent with the findings from ESCRT-dependent interphase nuclear envelope repair where no such trans-nuclear envelope microtubules exist [7-9]. These data link ESCRT-III assembly during mitotic exit to classical cell cycle control mechanisms and identify mitotic phosphorylation of CHMP7 as a mechanism to directly suppress this assembly.

Author Contributions

Conception and design: JGC. Acquisition, analysis, interpretation of data: JGC, CLS, ATG and YO. Drafting and revising manuscript: JCG, ATG and YO.

Acknowledgements

JCG is a Wellcome Trust Senior Research Fellow (206346/Z/17/Z), CLS is a BBSRC LIDO PhD student. This work was supported by the Francis Crick Institute which receives its core funding from Cancer Research UK (FC001002), the UK Medical Research Council (FC001002) and the Wellcome Trust (FC001002). We thank Prof Buzz Baum (UCL) for helpful discussion.

Figure Legends

Figure 1: ESCRT-III controls LEM2 dynamics during nuclear envelope reformation

A, B. HeLa cells stably expressing both GFP-CHMP7 and LEM2-mCh (A) or GFP-CHMP7 and treated with LEM2-targetting siRNA (B) were imaged live during mitotic exit. Images representative of 4/4 (GFP-CHMP7, LEM2-mCh) or 9/9 (LEM2-siRNA) movies analysed. C, D. HeLa cells stably expressing LEM2-mCh were treated with Control or CHMP7-targetting siRNA and imaged live during mitotic exit. LEM2-mCh fluorescence levels in a ROI around the chromatin were quantified in D from 25 (Control) or 18 (CHMP7 siRNA-1) or 14 (CHMP7 siRNA-2) individually imaged cells acquired over 3 independent experiments, mean ± S.E.M. presented. Significance was calculated using a 1-way ANOVA, with Dunnetts post-hoc test, $P < 0.0001$ in both cases. E-F. HeLa cells stably expressing LEM2-mCh were treated with Control or CHMP7-targetting siRNA, fixed and processed for immunofluorescence. The number of cells displaying aberrant LEM2 assemblies during cytokinesis or in interphase were quantified from 300 cells per condition, examined over 3 independent experiments. Significance was calculated using a 1-way ANOVA, with Dunnetts post-hoc test; CHMP7 siRNA-1 $P < 0.0001$ (interphase), $P = < 0.0001$ (cytokinesis); CHMP7 siRNA-2 $P = 0.0001$ (interphase), $P = < 0.0001$ (cytokinesis); IST1 siRNA $P = 0.456$ (interphase, n.s.), $P = 0.765$ (cytokinesis, n.s.). In all panels, time in minutes and a scale bar of 10 μm are reported.

Figure 2: Deletion of a regulatory helix in CHMP7's C-terminus decouples its assembly from the nuclear envelope during mitotic exit and causes inappropriate sequestration of LEM2 in interphase.

A. HeLa cells expressing GFP-CHMP7 δHelix6 were imaged live during mitotic exit (A) or imaged live, fixed and stained with antisera against IST1 and reimaged (B). Extra-nuclear envelope polymerisation of GFP-CHMP7 δHelix6 observed in 14/15 movies acquired (A) and co-localisation observed with endogenous IST1 in 4/4 correlative live and fixed cell imaging attempts (B). C. HeLa cells expressing LEM2-mCh and GFP-CHMP7 δHelix6 were imaged live during mitotic exit. Images representative of 4/4 movies acquired. D. HeLa cells or HeLa cells stably expressing LEM2-mCh expressing GFP-CHMP7 δHelix6 were fixed. Removal of LEM2-mCh from the INM and its sequestration in clusters observed in 18/18 imaged cells. E. GFP-tagged proteins were immunoprecipitated from 293T cells co-expressing HA-CHMP4B. Inputs and captured fractions were examined by western blotting with antisera raised against GFP or HA (N = 4). F. Recombinant CHMP7 was incubated with or without an equimolar concentration of recombinant $LEM2^{CT}$. Polymeric and soluble CHMP7, $LEM2^{CT}$, and CHMP7-$LEM2^{CT}$ complexes were recovered from pellet (P) and supernatant (S) fractions respectively, resolved by SDS-PAGE and analysed by Coomassie stain. Data presented a mean ± S.D., N = 6, $P = 0.0005$ by 2-tailed T-test. In all panels, time in minutes and a scale bar of 10 μm are reported.

Figure 3: CHMP7 is phosphorylated by CDK1 upon mitotic entry

A, B. HeLa cells expressing GFP-CHMP7 δHelix6 were imaged live (A) and the intensity of GFP-CHMP7 δHelix6 puncta were quantified during M-phase (B), quantification of 59 cells from 9 experiments.

Fluorescence traces normalised to metaphase onset (open arrowhead); nuclear envelope breakdown indicated by closed arrowhead. C. Lysates of HeLa cells stably expressing GFP-CHMP7 and subject to the indicated synchronisations were immunoprecipitated using GFP-trap resin and resolved using normal or Phos-tag SDS-PAGE. Inputs and captured fractions were examined by western blotting with antisera raised against GFP, or CDK1 substrate consensus sequences ([K/H]-[pS]-[P] or [pS]-[P]-[X]-[R/K]). Western blots representative of 6 Phos-tag immunoprecipitations. D. Lysates of HeLa cells stably expressing GFP-CHMP7 or GFP-CHMP7 S3A, S441A and subject to the indicated synchronisations were immunoprecipitated using GFP-trap resin and resolved using normal or Phos-tag SDS-PAGE. Inputs and captured fractions were examined by western blotting with antisera raised against GFP, Histone H3 pSer10 or GAPDH (N = 3). E-F. CAL-51 cells homozygously edited to express mNG-CHMP7 (E) or HeLa cells stably expressing LEM2-mCh (F) were synchronised to M-phase with STLC and then released from M through addition of RO-3306. Cells were imaged live through synchronised M-exit. G. Quantification of mNG-CHMP7$^{+/+}$ (onset 16.3 ± 0.88 mins; duration 3.1 ± 0.44 mins; N = 9, n = 104) or LEM2-mCh (onset 16.2 ± 2.22 mins; duration 4.1 ± 0.44 mins; N = 3, n = 80) assembly onset and duration time post RO3306 release from E and F. Additional quantification of the above parameters including HeLa cells stably expressing GFP-CHMP7 (onset 16.9 ± 1.21 mins; duration 3.3 ± 0.13 mins; N = 3, n = 97) and subject to STLC arrest and RO3306 release (from Figure S3E) and CAL-51 cells homozygously edited to express mNG-CHMP7 (onset 16.1 ± 2.02 mins; duration 4.2 ± 2.19 mins; N = 7, n = 39) and subject to nocodazole arrest and RO3306 release (from Figure S3F and Figure S3G). A 1-way ANOVA with Tukey's multiple comparisons revealed no significant differences between the datasets. H, I. HeLa cells stably expressing GFP-CHMP7^{NT} (H) or GFP-CHMP7 (I) were either untreated, or arrested in mitosis through STLC inhibition and forced out of mitosis using RO3306 for the indicated times. Lysates in H were resolved by normal or Phos-tag SDS-PAGE and examined with antisera raised against GFP or GAPDH. Lysates from I were immunoprecipitated using GFP-trap resin and both inputs and captured fractions were examined by western blotting with antisera raised against phosphorylated CDK1 substrates and GFP (N = 3). In all panels, time in minutes and a scale bar of 10 μm are reported.

Figure 4: CDK phosphorylation suppresses CHMP7 polymerisation and inappropriate capture of LEM2 during mitotic exit

A, B. Endogenous CHMP7 was depleted from HeLa cells stably expressing GFP-CHMP7^{R} S3A, S441A. Cells were either fixed and stained with antisera raised against IST1 or CHMP4B (A) and the number of cells exhibiting ESCRT-III puncta were quantified (B. Interphase; N = 4, n = 382 cells (GFP-CHMP7^{R}); N = 4, n = 697 cells (GFP-CHMP7^{R} S3A, S441A); P = 0.002, 2-tailed T-test. Mitosis, N = 3, n = 94 (GFP-CHMP7^{R}); N – 4, n = 80 (GFP-CHMP7^{R} S3A, S441A); P = 0.03, 2-tailed T-test. Data presented as mean ± S.D.). C. HeLa cells stably expressing either GFP-CHMP7^{R} or GFP-CHMP7^{R} S3A, S441A were transfected with siRNA targeting CHMP7 and imaged during mitotic exit. Arrowheads depict precocious polymerisation of CHMP7 in the peripheral ER during anaphase that develop during mitotic exit. Images representative of greater than

20 imaged cells in each case. D. Recombinant CHMP7 was incubated with recombinant CDK1 and CCNB1 in the presence or absence of ATP. Polymeric and soluble CHMP7 was recovered from pellet and supernatant fractions respectively, resolved by Phos-tag SDS-PAGE and analysed by western blotting using antisera raised against CHMP7. Data presented as mean ± S.D., N = 4, P = 0.0007 by paired 2-tailed T-test. E. HeLa cells stably expressing LEM2-mCh and either GFP-CHMP7^{R} or GFP-CHMP7^{R} S3A, S441A were transfected with siRNA targeting CHMP7 and imaged during mitotic exit. Precocious clusters were observed in 15/49 (WT) and 12/15 (S3A, S441A) imaged cells. In all panels, time in minutes and a scale bar of 10 μm is depicted.

Figure S1. Activities within LEM2 controlling its assembly at the nuclear envelope.

A. HeLa cells stably expressing LEM2-mCh or LEM2$^{\delta LEM}$-mCh were lysed, resolved by SDS-PAGE and analysed by western blotting with anti-LEM2 or anti-GAPDH antisera (endogenous LEM2, LEM2-mCh or LEM2$^{\delta LEM}$-mCh indicated by arrow, open arrowhead or closed arrowhead respectively. Alternatively, cells were imaged live. Images of LEM2$^{\delta LEM}$-mCh representative of 35/40 cells. B. Cells from A were imaged during mitosis. In addition to a failure to enrich at the reforming nuclear envelope, note the failure of LEM2$^{\delta LEM}$-mCh to be retained at the INM (open arrowheads) relative to the peripheral ER (closed arrowheads). Images representative of 8/9 imaged cells. C. HeLa cells stably expressing GFP-CHMP7 and LEM2$^{\delta LEM}$-mCh were imaged live through mitosis. Arrowheads indicated inappropriate extra-nuclear polymerisation of GFP-CHMP7 and LEM2$^{\delta LEM}$-mCh. Note the limited NE enrichment of LEM2$^{\delta LEM}$-mCh during nuclear envelope reformation and its sequestration in extranuclear clusters at the end of mitosis, rather than at the INM. D. HeLa cells stably expressing LEM2-mCh or LEM2$^{\delta 415-485}$-mCh were scored for nuclear morphology and LEM2 clustering defects. Mean ± S.D. from 3 independent experiments (LEM2-mCh, n = 775; LEM2$^{\delta 415-485}$-mCh, n = 1009). Statistical differences between the two lines were analysed by an unpaired 2-tailed T-test; nuclear envelope clusters, P = 0.0003; nuclear envelope folds, P = 0.0007. E. HeLa cells stably expressing LEM2-mCh were treated with Control or IST1-targetting siRNA and imaged live during mitotic exit. LEM2-mCh fluorescence levels in a ROI around the chromatin were quantified from 25 (Control) or 11 (IST1 siRNA) individually imaged cells. Significance was calculated using an unpaired 2-tailed T-test, P = 0.528, mean ± SD presented. F, G. HeLa cells stably expressing LEM2-mCh were treated with control or CHMP7-1 targeting siRNA, fixed and stained with antisera raised against LAP1 or Emerin. Images representative of > 20 imaged cells in each case. H. HeLa cells stably expressing LEM2-mCh were transfected with Control, CHMP7-1, CHMP7-2 or IST1 siRNA, fixed and stained with antisera raised against HP1. Maximum projection and single slices of the HP1 channel were presented. I. Quantification of data from H. HP1 foci per cell were scored from 3 independent experiments (Control, n = 297; CHMP7-1, n = 298; CHMP7-2, n = 311; IST1, n = 165). Mean ± S.E.M. presented. Significance was calculated using a 1-way ANOVA, with Dunnetts post-hoc test, P = 0.013 (CHMP7-1), P = 0.010 (CHMP7-2), P = 0.894 (IST1). J. Separation of

data from CHMP7-depleted cells in I into cells with or without LEM2 clusters. In all panels, time in minutes and a scale bar of 10 μm is depicted.

Figure S2: Nuclear export sequences within CHMP7's C-terminus protect against unregulated exposure to LEM2

A. Sequence alignment of CHMP7 Helix 5 and Helix 6 across phyla. Hs, *Homo sapiens*; Mm, *Mus musculus*; Dr, *Danio rerio*; Dm, *Drosophila melanogaster*; Dd, *Dictyostelium discoideum*; Sc, *Saccharomyces cerevisiae*. Type-1 Nuclear Export Sequence (NES) and MIM1 consensus sequence presented underneath; charge substituted residues in mammalian CHMP7 MIM1 indicated by asterisks. B. HeLa cells were transfected with the indicated GFP-tagged C-terminal fragments of CHMP7 with mutations in the NES in Helix 5 (L380A, L384A, L387A) or Helix 6 (L421A, L425A, L428A) and imaged. C. Nucleocytoplasmic fluorescence intensities of the indicated constructs were quantified from B. Data presented as mean ± S.E.M. from N = 3 independent experiments. Statistical significance was calculated using a 1-way ANOVA with Tukey's multiple comparison. (GFP, n = 44; GFP-CHMP7 393-CT, n = 72; GFP-CHMP7 393-CT α6 LLL-AAA, n = 90; GFP-CHMP7 377-CT, n = 106; GFP-CHMP7 377-CT α6 LLL-AAA, n = 125; GFP-CHMP7 377-CT α5 LLL-AAA + α6 LLL-AAA, n = 99; **** $P < 0.0001$). D. HeLa cells stably expressing GFP-CHMP7 were treated with Leptomycin B for the indicated time, fixed and imaged. Data presented as mean ± S.E.M from 3 independent experiments. Statistical significance was calculated with an unpaired 2-tailed T-test, $P = 0.05$; n = 13 (Control), n = 14 (LMB). E. HeLa cells were transfected with plasmids encoding GFP-tagged C-terminal fragments of CHMP7 with mutations in the NES in Helix 6 (GFP-CHMP7^{NES-}) or Helix 5 and Helix 6 (GFP-CHMP7^{2xNES-}). Data presented as mean ± S.E.M. from N = 3 independent experiments, GFP-CHMP7 n = 83; GFP-CHMP7^{NES-}, n = 107; GFP-CHMP7^{2xNES-}, n = 189. Localisation was binned into 4 categories: Normal ER localisation, sub-ER nuclear localisation, supra-ER nuclear localisation and clusters; the majority of clusters were detected inside the nucleus (arrow) with occasional detection outside the nucleus (arrowhead). Statistical significance was calculated using a 1-way ANOVA with Dunnett's multiple comparison, **** $P < 0.0001$. F. HeLa cells stably expressing LEM2-mCh were transfected with plasmids encoding GFP-CHMP7, GFP-CHMP7^{NES-}, GFP-CHMP7^{2xNES-} and imaged live. G. HeLa cells were transfected with plasmids expressing GFP-CHMP7^{2xNES-} and stained with antisera raised against PML (n = 27 cells from N = 2 independent experiments). H. HeLa cells stably expressing LEM2-mCh were fixed 48 hours after transduction with retrovirus packaging GFP-CHMP7^{2xNES-} (n = 55 cells from N = 2 independent experiments). I. HeLa cells transfected with CHMP7-targetting siRNA and transiently expressing GFP-CHMP7^{R} or GFP-CHMP7^{R} δHelix6 were fixed, stained with DAPI and imaged. GFP-CHMP7^{R} δHelix6 was poorly exported from the nucleus, assembled aberrantly in the cytoplasm (arrowheads) and was not clearly enriched at the nuclear envelope (arrow). J. Nucleocytoplasmic ration of GFP-CHMP7 or GFP-CHMP7 δHelix6 was quantified Data presented as mean ± S.E.M from 3 independent experiments. Statistical significance was calculated with an unpaired 2-tailed T-test, $P = 0.023$; n = 20 (WT), n = 117 (δHelix6). K. Glutathione-

sepharose captured fractions and lysates from 293T cells transiently expressing YFP-VPS4^{MIT} and either GST, GST-CHMP7 393-CT, GST-CHMP7 393-CT+MIM, or GST-CHMP7 393-CT ES-RR were examined by western blotting with antisera raised against GST or GFP (N = 3) and quantified by infrared imaging (N = 2). Mean ± S.D. presented, P-values generated with 1-way ANOVA with Tukey's multiple comparison. CHMP7 393-CT + MIM contained the CHMP2A MIM inserted in place of Helix 6 and allowed binding to YFP-VPS4^{MIT} (P = 0.038). CHMP7 393-CT ES-RR (E424R, S429R) was created to restore the Type-1 MIM and permitted binding to YFP-VPS4^{MIT} (P = 0.003). L. Glutathione-sepharose captured fractions and lysates from 293T cells transiently expressing HA-CHMP4B and GST-CHMP7 or GST-CHMP7 δHelix6 were examined by western blotting with antisera raised against GST or HA (N = 2). In all panels, time in minutes and a scale bar of 10 μm is depicted.

Figure S3: Mapping mitotic phosphorylation of CHMP7 to Ser3 and Ser441

A. 293T cells expressing the indicated GFP-CHMP7 constructs were cultured asynchronously or synchronised in mitosis through Eg5 inhibition. GFP-tagged proteins were immunoprecipitated and examined by western blotting with antisera raised against GFP and the CDK1 substrate consensus sequences [K/H]-[pS]-[P]. N = 3. B. HeLa cells stably expressing GFP-CHMP7 393-CT or GFP-CHMP7 393-CT S441A were cultured asynchronously or synchronised at mitosis through Eg5 inhibition, then were lysed, resolved by normal or Phos-tag SDS-PAGE and examined by western blotting with antisera raised against GFP or GAPDH (N = 3). C, D. 293T cells expressing the indicated GFP-CHMP7^{NT} proteins were cultured asynchronously or synchronised in mitosis via Eg5 inhibition, then were lysed, resolved by normal or Phos-tag SDS-PAGE and examined by western blotting with antisera raised against GFP or GAPDH (N = 3). In C, Ser/Thr containing mutants selected from a previously generated panel of alanine-scanning GFP-CHMP7^{NT} mutations [3] were assessed for a mobility shift in mitosis. Mobility shift was compromised by M1, M27 and M28, although M27 and M28 were poorly expressed. M1 encodes the mutations W2A, S3A, P4A, E5A; M27 encodes the mutations R106A, E107A, S108A, D109A; M28 encodes the mutations F110A, M111A, A112G, S113A. individual mutations of S3A, S108A and S113A from M1, M27 and M28 were examined in Figure S3D, revealing the site of phosphorylation to be Ser 3. E. HeLa cells stably expressing GFP-CHMP7^{R} and treated with CHMP7 siRNA were synchronised to M-phase with STLC and then released from M through addition of RO-3306. Cells were imaged live through synchronised M-exit. Data were quantified in Figure 3G. F, G. CAL-51 cells homozygously edited to express mNG-CHMP7 were synchronised to M-phase with nocodazole and then released from M through addition of RO-3306. Cells were imaged live through synchronised M-exit. Note persistent assembly in the absence of microtubules (G, Recruitment observed in 245/258 cells (N = 3).) and furrow-proximal initiation of assembly in 13/14 cells forming a pseudofurrow (F). H. HeLa cells stably expressing LEM2-mCh were transfected with Control or CHMP7-1 siRNA, arrested in mitosis with STLC and released via RO3306 treatment. I. Cells from H were fixed, stained with antisera raised against Tubulin and imaged. The percentage of cells displaying LEM2-mCh clusters at the indicated time after RO3306 release

was quantified (Control siRNA, 30 minutes post RO3306 release, N = 8, n = 92; CHMP7 siRNA, 30 minutes post RO3306 release, N = 9, n = 98; CHMP7 siRNA 60 minutes post RO3306 release, N = 9, n = 98. Significance was calculated using a 1-way ANOVA with Tukey's multiple comparisons, **** $P < 0.0001$. J. CAL-51 cells homozygously edited to express mNG-CHMP7 were synchronised to M-phase with STLC and then released from M through addition of RO-3306 in the presence of Calyculin A (100 nM) or Okadaic Acid (1 μM). Control, N = 6, n = 263; Calyculin A, N = 4, n = 162; Okadaic Acid, N = 4, n = 249. In all panels, time in minutes and a scale bar of 10 μm is depicted.

Figure S4: CDK phosphorylation suppresses CHMP7 polymerisation and inappropriate capture of LEM2 during mitotic exit

A.HeLa cells stably expressing either GFP-CHMP7^{R} or GFP-CHMP7^{R} S3A, S441A were imaged during mitosis. Arrowheads depict precocious polymerisation of GFP-CHMP7^{R} S3A, S441A in the peripheral ER. Quantification in Figure 4B. B-D. HeLa cells stably expressing LEM2-mCh and either GFP-CHMP7^{R} or GFP-CHMP7^{R} S3A, S441A were transfected with siRNA targeting CHMP7 and imaged during mitotic exit. Arrowheads in B depict precocious polymerisation of LEM2-mCh and GFP-CHMP7^{R} S3A, S441A in the peripheral ER. Precocious clusters of LEM2-mCh and GFP-CHMP7^{R} were observed in 9/31 imaged movies Precocious clusters of LEM2-mCh and GFP-CHMP7^{R} S3A, S441A were observed in 7/9 imaged movies. In C, an example of fusogenic behaviour of the LEM2-mCh and GFP-CHMP7 S3A, S441A positive clusters is shown, leading to the generation of a singular LEM2-mCh and GFP-CHMP7 S3A, S441A positive cluster, depicted in D. In all panels, time in minutes and a scale bar of 10 μm is depicted.

Movie Legends

Movie 1. Related to Figure 1A. HeLa cells stably expressing GFP-CHMP7 and LEM2-mCh were imaged through mitotic exit.

Movie 2. Related to Figure 1B. HeLa cells stably expressing GFP-CHMP7 were treated with LEM2 siRNA were imaged through mitotic exit.

Movie 3. Related to Figure S1B. HeLa cells stably expressing LEM2-mCh or LEM2$^{\delta LEM}$-mCh were imaged through mitotic exit.

Movie 4. Related to Figure 1C and 1B. HeLa cells stably expressing LEM2 and treated with the indicated siRNA were imaged through mitotic exit.

Movie 5. Related to Figure 2A. HeLa cells expressing GFP-CHMP7$^{\delta Helix6}$ were imaged throughout mitotic exit.

Movie 6. Related to Figure 3A. HeLa cells expressing GFP-CHMP7$^{\delta Helix6}$ were imaged throughout mitotic exit.

Movie 7. Related to Figure 3E. CAL-51 mNG-CHMP7$^{+/+}$ were released from an STLC-induced mitotic arrest using RO3306.

Movie 8. Related to Figure S3E. HeLa cells stably expressing GFP-CHMP7^{R} and transfected with CHMP7 siRNA were released from an STLC-induced mitotic arrest using RO3306.

Movie 9. Related to Figure 3F. HeLa cells stably expressing LEM2-mCh were released from an STLC-induced mitotic arrest using RO3306.

Movie 10. Related to Figure S3F. CAL-51 mNG-CHMP7$^{+/+}$ cells were released from a nocodazole-induced mitotic arrest using RO3306.

Movie 11. Related to Figure S3G. CAL-51 mNG-CHMP7$^{+/+}$ cells were released from a nocodazole-induced mitotic arrest using RO3306.

Movie 12. Related to Figure S3H. HeLa cells stably expressing LEM2-mCh and transfected with control or CHMP7 siRNA-1 were released from an STLC-induced mitotic arrest using RO3306.

Movie 13. Related to Figure 4C. HeLa cells stably expressing GFP-CHMP7^{R} or GFP-CHMP7^{R} S3A, S441A were transfected with CHMP7 siRNA-1 and were imaged live during mitotic exit.

Movie 14. Related to Figure 4E. HeLa cells stably expressing LEM2-mCh and GFP-CHMP7^{R} S3A, S441A and transfected with CHMP7 siRNA-1 were imaged live during mitotic exit.

Movie 15. Related to Figure S4C and S4D. HeLa cells stably expressing LEM2-mCh and GFP-CHMP7^{R} S3A, S441A and transfected with CHMP7 siRNA-1 were imaged live.

Experimental Procedures

Cell Culture

STR-profiled, mycoplasma-free vials of HeLa, 293T, GP2-293 and CAL-51, CAL-51-mNG-CHMP7$^{+/+}$ cells have been described previously [3] and were banked and obtained from the Crick Cell Services Science Technology Platform. Cells were cultured in DMEM containing 10% FBS, Penicillin (100 U/ml) and Streptomycin (0.1 mg/ml). Stable cells lines were generated by transduction using MLV-based retroviruses as described previously [1], and selected using Puromycin (1 μg/ml) or G418 (750 μg/ml) as necessary. Where necessary, cells were sorted to monoclonality by limiting dilution or FACS. Cell lines stably expressing GFP-CHMP7^{R} have been described previously [3].

Plasmids

Retroviral expression vectors containing the human CHMP7 coding sequence (both WT and siRNA-resistant and N-terminal scanning mutagenesis) have been described previously [3]. A codon optimised human LEM2 sequence was obtained by genesynthesis (GeneWIZ) and cloned *EcoRI-NotI* into a modified version of pMSCVneo bearing an *EcoRI-NotI-XhoI* polylinker leading into mCherry. Derivatives and mutations of CHMP7 and LEM2 were obtained by standard molecular biology protocols and cloned into pCMS28-GFP-CHMP7 or pMSCVneo LEM2-mCh as required. For expression of recombinant proteins, the open reading frames of full length CHMP7 and LEM2 C-terminal domain 395-503 (LEM2^{CT}) were cloned *EcoRI-NotI* into a version of pET28a comprising N-terminal tandem His$_6$ affinity tag, an N-utilisation sequence A (NusA) solubilisation tag [24], and a TEV-recognition site that cleaves at the 1st Methionine.

Generation of stable cell lines

For retroviral transduction, above constructs in retroviral packaging vectors were transfected with pVSVG into GP2-293 cells (Clontech). Supernatants were harvested, clarified by centrifugation (200 x g, 5 minutes), filtered (0.45 μm) and used to infect target cells in the presence of 8 μg/ml polybrene (Millipore) at MOI < 1. Antibiotic selection was applied after 48 hours.

Antibodies

An antibody against GAPDH (MAB374) was from Millipore; Calnexin (ab22595) was from Abcam; Tubulin (DM1A) was from Sigma; CHMP2A (10477-1-AP) was from Proteintech; IST1 (51002-1-AP) was from Proteintech; CHMP7 (16424-1-AP) was from Proteintech. GFP (7.1/13.1) was from Roche; mCherry (ab167453) was from Abcam. Anti-CDK1 substrate antibodies were from Cell Signaling Technology (9477S and 2325S). Anti-Histone H3 pS10 was from Cell Signaling Technology (9701S). Alexa555-conjugated anti PML was from Abcam (ab217524). Alexa conjugated secondary antibodies were from Invitrogen and HRP-conjugated secondary antibodies were from Millipore. IRDye 800 CW (925-32210) and IRDye 680 RD (925-68071) were from LI-COR Biosciences.

SDS-PAGE and western blotting

Cell lysates and fractions were denatured by boiling in denaturing LDS-sample buffer (Life Technologies) and resolved using SDS-PAGE using precast Novex gels (Life Technologies). Resolved proteins were transferred onto nitrocellulose by western blotting (wet transfer, 100V, 1h) and were probed with the indicated antisera in 5% milk or BSA. HRP-conjugated secondary antibodies were used to probe membranes, following by incubation with ECL Prime enhanced chemiluminescent substrate (GE Healthcare) and visualized by exposure to autoradiography film; alternatively, IRdye fluorophore conjugated secondary antibodies were used to probe membranes, following by visualisation by infrared imaging (LICOR Odyssey Fc). Where necessary, 10% polyacrylamide gels were prepared manually containing 200 μM $MnCl_2$ and either 25 μM Phos-tag-acrylamide (whole cell lysates) or 50 μM Phos-tag-acrylamide (immunoprecipitants). Phos-tag-acrylamide was from Fujifilm Wako Chemicals. EDTA-free Lamelli buffer was used to prepare lysates for Phos-tag-gels, prestained molecular weight markers (NEB) were supplemented with twice the volume of 10 mM $MnCl_2$ and 1 volume of 4x EDTA-free Lamelli buffer. After electrophoresis, Phos-tag gels were soaked for 10 minutes in Tris-Gly transfer buffer containing 10 mM EDTA, 10 minutes in Tris-Gly transfer buffer containing 1 mM EDTA and 10 minutes in Tris-Gly transfer buffer prior to electro-transfer.

Transient transfection of cDNA

HeLa and CAL-51 cells were transfected using Lipofectamine-3000 (Life Technologies) according to the manufacturer's instructions. 293GP2 cells were transfected using linear 25-kDa polyethylenimine (PEI, Polysciences, Inc.), as described previously [25].

siRNA transfections

HeLa cells were seeded at a density of 1E5 cells/ml and were transfected with siRNA at 20 nM, 2 hours after plating using RNAi-MAX (Invitrogen), for 72 hours. The following targeting sequences that have previously been demonstrated to achieve potent and specific suppression of the targeted CHMP were employed: Control, Dharmacon Non-targeting control D-001810; CHMP7-1 (GGGAGAAGATTGTGAAGTTdTdT), CHMP7-2 (GGAGGUGUAUCGUCUGUAUdTdT); LEM2 and IST1, siGenome Dharmacon SmartPools.

Recombinant proteins

Both CHMP7 and $LEM2^{CT}$ were purified as previously described [4,6] with some modifications. *Escherichia coli* BL21(DE3) cells expressing the $2xHis_6$-NusA-TEV-tagged proteins were grown at 37°C to OD 0.6 in LB medium, transferred to 18°C and induced with 0.25 mM IPTG overnight. Cells expressing full length CHMP7 were harvested by centrifugation and lysed with TNG1000 lysis buffer (50 mM Tris-HCl, 1 M NaCl, 10% w/v Glycerol, pH 7.5) supplemented with 1 tablet of cOmplete Protease Inhibitors (Roche), 20 mM imidazole, 5 mM β-ME, 0.2% Triton X-100, 1 mM PMSF, 10 μg/ml DNaseI, and 1 mg/ml lysozyme. Cells were then

sonicated and clarified by centrifugation at 40,000 × *g* for 60 min. Supernatants were incubated with Ni-NTA beads at 4°C for 2 hours. Beads were extensively washed with complete TNG1000 lysis buffer, transferred into a TNG1000 buffer with 0.01% Triton X-100, and eluted in four steps of this buffer containing stepwise increasing imidazole concentrations (50, 150, 250, and 400 mM). The eluted protein was dialyzed overnight against size exclusion (SEC) buffer (50 mM Tris-HCl, 150 mM NaCl, 0.5 mM TCEP, 5% glycerol, pH 7.6) in the presence of recombinant TEV protease. The sample was further dialysed for two more times in fresh SEC buffer, before incubating with new Ni-NTA beads for re-capturing the 2xHis_6-NusA tag. The supernatant was then injected into a Superdex 200 Increase 10/300 GL column pre-equilibrated with SEC buffer, monomeric CHMP7 fractions were pulled, aliquoted and snap-frozen in liquid nitrogen. Yield was 1 mg of protein per 4 L of bacterial culture. BL21(DE3) cells expressing $LEM2^{CT}$ were processed similarly, with some modifications: lysis and washes were carried out in TNG500 lysis buffer (50 mM Tris-HCl, 500 mM NaCl, 10% w/v Glycerol, pH 7.5); no stepwise imidazole elution was performed; TEV cleavage was achieved on the Ni-bound protein during the overnight dialysis. Fractions containing $LEM2^{CT}$ were pulled, concentrated, aliquoted and snap-frozen in liquid nitrogen. Yield was 4 mg of protein per 3 L of bacterial culture. Before subsequent experiments, proteins were thawed quickly and cleared by centrifugation at 22,000 × *g* for 20 min.

CHMP7-LEM2 sedimentation assay

10 μM CHMP7 was incubated with equimolar concentration of $LEM2^{CT}$ by diluting the proteins in sedimentation (SED) buffer (50 mM Tris-HCl, 150 mM NaCl, 0.5 mM TCEP, pH 7.6). After 60 min incubation at 30°C, samples were spun in a benchtop centrifuge at 22,000 × *g* for 40 min at 4°C. Supernatant (S) and Pelleted (P) fractions were resuspended in equal volumes of 1x Lamelli buffer, run on an SDS-PAGE gel and analysed by Coomassie staining. Band intensities were quantified by densitometry using ImageJ and ratios of insoluble pelleted proteins were calculated.

Fixed cell imaging

HeLa cells were fixed in MeOH or 4% PFA and subject to processing for immunofluorescence as described previously. Cells were imaged using a Nikon Eclipse microscope teamed with an Andor Dragonfly 200 Spinning Disc Confocal imaging system and paired with Andor Zyla sCMOS and Andor iXon EM-CCD cameras. Images were processed in FIJI and exported to Photoshop for assembly into figures.

Live cell imaging

Cells stably expressing the indicated proteins, or edited to express fluorescent proteins, were plated in 4- or 8-chamberslides (Ibidi). Cells were transfected with the indicated siRNA where necessary. Cells were transferred to an inverted Nikon Eclipse microscope teamed with an Andor Dragonfly 200 Spinning Disc Confocal unit and paired with Andor Zyla sCMOS and Andor iXon EM-CCD cameras, with attached environmental chamber (Oxolabs) and imaged live using 20x dry or 60x oil-immersion objectives, typically

acquiring frames every 30 seconds. In all cases, 405, 488 or 561 laser lines were used for illumination. To enable multifield overnight imaging, movies were acquired using a x20 dry objective, preventing resolution of GFP-CHMP7 δHelix6 localisation to the ER or assembly in fine puncta, as per Figure 3A. For monopolar spindle assays, cells were incubated for 16h with S-trityl L-cystine (5 μM) or Nocodazole (50 ng/ml) to arrest cells in M-phase. Cells were released from M-phase through addition of the CDK1 inhibitor RO-3306 to a final concentration of 9 μM. Cells were either imaged live, or were collected for biochemical experiments as described below.

Immunoprecipitation

Cells were lysed on ice in RIPA buffer (150 mM NaCl, 50 mM Tris-Cl pH 7.4, 1% NP-40, 0.2 % SDS, 0.5% Sodium deoxycholate) supplemented with protease (HALT, Sigma) and phosphatase (PhosSTOP, Roche) inhibitor cocktails. Clarified lysates were incubated with GFP-trap magnetic agarose beads (Chromotek) for 1 hour, washed thrice using Pulldown Wash buffer (150 mM NaCl, 50 mM Tris-Cl pH 7.4, 0.1% NP-40) after magnetic capture, and released from the resin through boiling in 2 x Laemlli buffer.

GST-pull down assay

293T cells expressing GST-tagged constructs were lysed on ice in Pulldown Lysis buffer (150 mM NaCl, 50 mM Tris-Cl pH 7.4, 1% NP-40) supplemented with protease inhibitor (HALT, Sigma) cocktail. Clarified lysates were incubated by glutathione sepharose 4β beads (GE healthcare) for 2 hours, washed thrice using Pulldown Wash buffer after centrifugal capture, and released from the resin through boiling in 2 x Laemlli buffer.

In vitro kinase assay

10 μM of recombinant CHMP7 was incubated in SED buffer (50 mM Tris-HCl, 150 mM NaCl, 0.5 mM TCEP, pH 7.6) with 10 mM $MgCl_2$, 1 μg of recombinant CDK1:CyclinB1 active complex (Millipore) in the presence or absence of 3 mM ATP. After 60 min at 30°C, samples were spun in a benchtop centrifuge at 22,000 × *g* for 40 min at 4°C. Supernatant (S) and Pelleted (P) fractions were resuspended in equal volumes of 1x Laemmli buffer, run on a Phos-tag SDS-PAGE gel. Samples and gels were prepared as described above. Western-blot band intensities were quantified by densitometry using ImageJ and ratios of insoluble pelleted proteins were calculated.

Statistical analysis

2-tailed Student's T-tests, or ordinary 1-way ANOVA with the indicated post-hoc tests were used to assess significance between test samples and controls and were performed using GraphPad Prism. N-numbers given as the number of independent experiments, n-numbers given as the number of cells analysed.

References

[1] Olmos Y, Hodgson L, Mantell J, Verkade P, Carlton JG. ESCRT-III controls nuclear envelope reformation. Nature 2015;522:236–9. doi:10.1038/nature14503.

[2] Vietri M, Schink KO, Campsteijn C, Wegner CS, Schultz SW, Christ L, et al. Spastin and ESCRT-III coordinate mitotic spindle disassembly and nuclear envelope sealing. Nature 2015;522:231–5. doi:10.1038/nature14408.

[3] Olmos Y, Perdrix-Rosell A, Carlton JG. Membrane Binding by CHMP7 Coordinates ESCRT-III-Dependent Nuclear Envelope Reformation. Curr Biol 2016;26:2635–41. doi:10.1016/j.cub.2016.07.039.

[4] Gu M, LaJoie D, Chen OS, Appen von A, Ladinsky MS, Redd MJ, et al. LEM2 recruits CHMP7 for ESCRT-mediated nuclear envelope closure in fission yeast and human cells. Proc Natl Acad Sci USa 2017;114:E2166–75. doi:10.1073/pnas.1613916114.

[5] Willan J, Cleasby AJ, Flores-Rodriguez N, Stefani F, Rinaldo C, Pisciottani A, et al. ESCRT-III is necessary for the integrity of the nuclear envelope in micronuclei but is aberrant at ruptured micronuclear envelopes generating damage. Oncogenesis 2019;8:29. doi:10.1038/s41389-019-0136-0.

[6] Appen von A, LaJoie D, johnson IE, Trnka M, Pick SM, Burlingame AL, et al. A role for liquid-liquid phase separation in ESCRT-mediated nuclear envelope reformation. bioRxiv 2019;39:577460. doi:10.1101/577460.

[7] Raab M, Gentili M, de Belly H, Thiam HR, Vargas P, Jimenez AJ, et al. ESCRT III repairs nuclear envelope ruptures during cell migration to limit DNA damage and cell death. Science 2016. doi:10.1126/science.aad7611.

[8] Denais CM, Gilbert RM, Isermann P, McGregor AL, Lindert Te M, Weigelin B, et al. Nuclear envelope rupture and repair during cancer cell migration. Science 2016. doi:10.1126/science.aad7297.

[9] Robijns J, Molenberghs F, Sieprath T, Corne TDJ, Verschuuren M, De Vos WH. In silico synchronization reveals regulators of nuclear ruptures in lamin A/C deficient model cells. Sci Rep 2016;6:30325. doi:10.1038/srep30325.

[10] Vietri M, Schultz SW, Bellanger A, Jones CM, Raiborg C, Skarpen E, et al. Unrestrained ESCRT-III drives chromosome fragmentation and micronuclear catastrophe. bioRxiv 2019:517011. doi:10.1101/517011.

[11] Webster BM, Thaller DJ, Jäger J, Ochmann SE, Borah S, Lusk CP. Chm7 and Heh1 collaborate to link nuclear pore complex quality control with nuclear envelope sealing. Embo J 2016:e201694574. doi:10.15252/embj.201694574.

[12] Webster BM, Colombi P, Jäger J, Lusk CP. Surveillance of Nuclear Pore Complex Assembly by ESCRT-III/Vps4. Cell 2014;159:388–401. doi:10.1016/j.cell.2014.09.012.

[13] Penfield L, Shankar R, Szentgyörgyi E, Laffitte A, Mauro MS, Audhya A, et al. Regulated lipid synthesis and LEM2/CHMP7 jointly control nuclear envelope closure. J Cell Biol 2020;219:15. doi:10.1083/jcb.201908179.

[14] Ikegami K, Egelhofer TA, Strome S, Lieb JD. Caenorhabditis elegans chromosome arms are anchored to the nuclear membrane via discontinuous association with LEM-2. Genome Biol 2010;11:R120–0. doi:10.1186/gb-2010-11-12-r120.

[15] Barrales RR, Forn M, Georgescu PR, Sarkadi Z, Braun S. Control of heterochromatin localization and silencing by the nuclear membrane protein Lem2. Genes Dev 2016;30:133–48. doi:10.1101/gad.271288.115.

[16] Pieper GH, Sprenger S, Teis D, Oliferenko S. ESCRT-III/Vps4 Controls Heterochromatin-Nuclear Envelope Attachments. Dev Cell 2020. doi:10.1016/j.devcel.2020.01.028.

[17] Lee I-J, Stokasimov E, Dempsey N, Varberg JM, Jacob E, Jaspersen SL, et al. Factors promoting nuclear envelope assembly independent of the canonical ESCRT pathway. J Cell Biol 2020;219:174. doi:10.1083/jcb.201908232.

[18] Thaller DJ, Allegretti M, Borah S, Ronchi P, Beck M, Lusk CP. An ESCRT-LEM protein surveillance system is poised to directly monitor the nuclear envelope and nuclear transport system. Elife 2019;8:33. doi:10.7554/eLife.45284.

[19] Schöneberg J, Lee I-H, Iwasa JH, Hurley JH. Reverse-topology membrane scission by the ESCRT proteins. Nat Rev Mol Cell Biol 2017;18:5–17. doi:10.1038/nrm.2016.121.

[20] Shim S, Kimpler LA, Hanson PI. Structure/function analysis of four core ESCRT-III proteins reveals common regulatory role for extreme C-terminal domain. Traffic 2007;8:1068–79. doi:10.1111/j.1600-0854.2007.00584.x.

[21] Hu C-K, Coughlin M, Field CM, Mitchison TJ. Cell polarization during monopolar cytokinesis. J Cell Biol 2008;181:195–202. doi:10.1083/jcb.200711105.

[22] Skoufias DA, DeBonis S, Saoudi Y, Lebeau L, Crevel I, Cross R, et al. S-trityl-L-cysteine is a reversible, tight binding inhibitor of the human kinesin Eg5 that specifically blocks mitotic progression. J Biol Chem 2006;281:17559–69. doi:10.1074/jbc.M511735200.

[23] Vassilev LT, Tovar C, Chen S, Knezevic D, Zhao X, Sun H, et al. Selective small-molecule inhibitor reveals critical mitotic functions of human CDK1. Proc Natl Acad Sci USa 2006;103:10660–5. doi:10.1073/pnas.0600447103.

[24] Davis GD, Elisee C, Newham DM, Harrison RG. New fusion protein systems designed to give soluble expression in Escherichia coli. Biotechnol Bioeng 1999;65:382–8.

[25] Carlton JG, Martin-Serrano J. Parallels between cytokinesis and retroviral budding: a role for the ESCRT machinery. Science 2007;316:1908–12. doi:10.1126/science.1143422.

Gatta, Olmos, Stoten, Figure 1

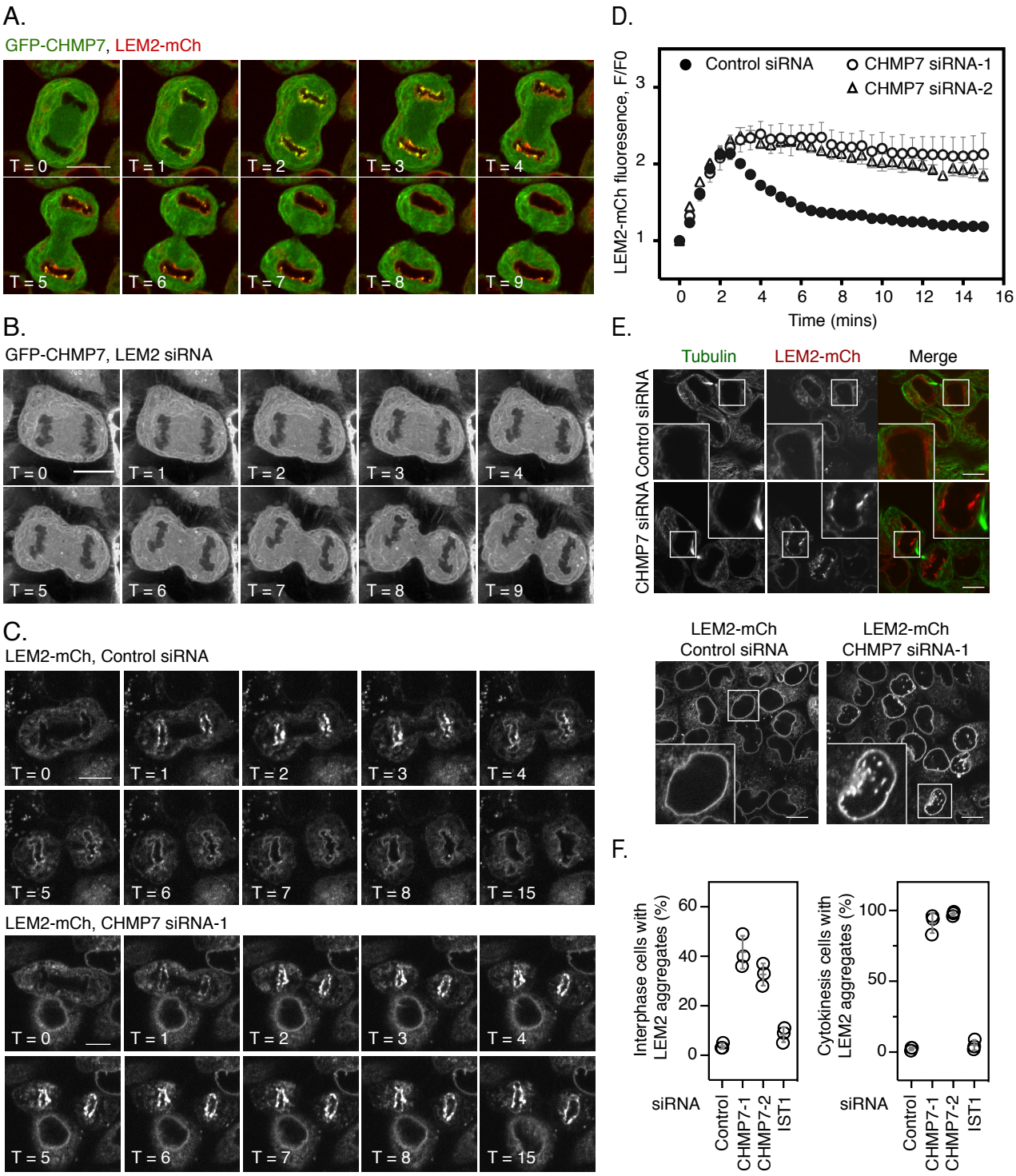

Gatta, Olmos, Stoten, Figure 2

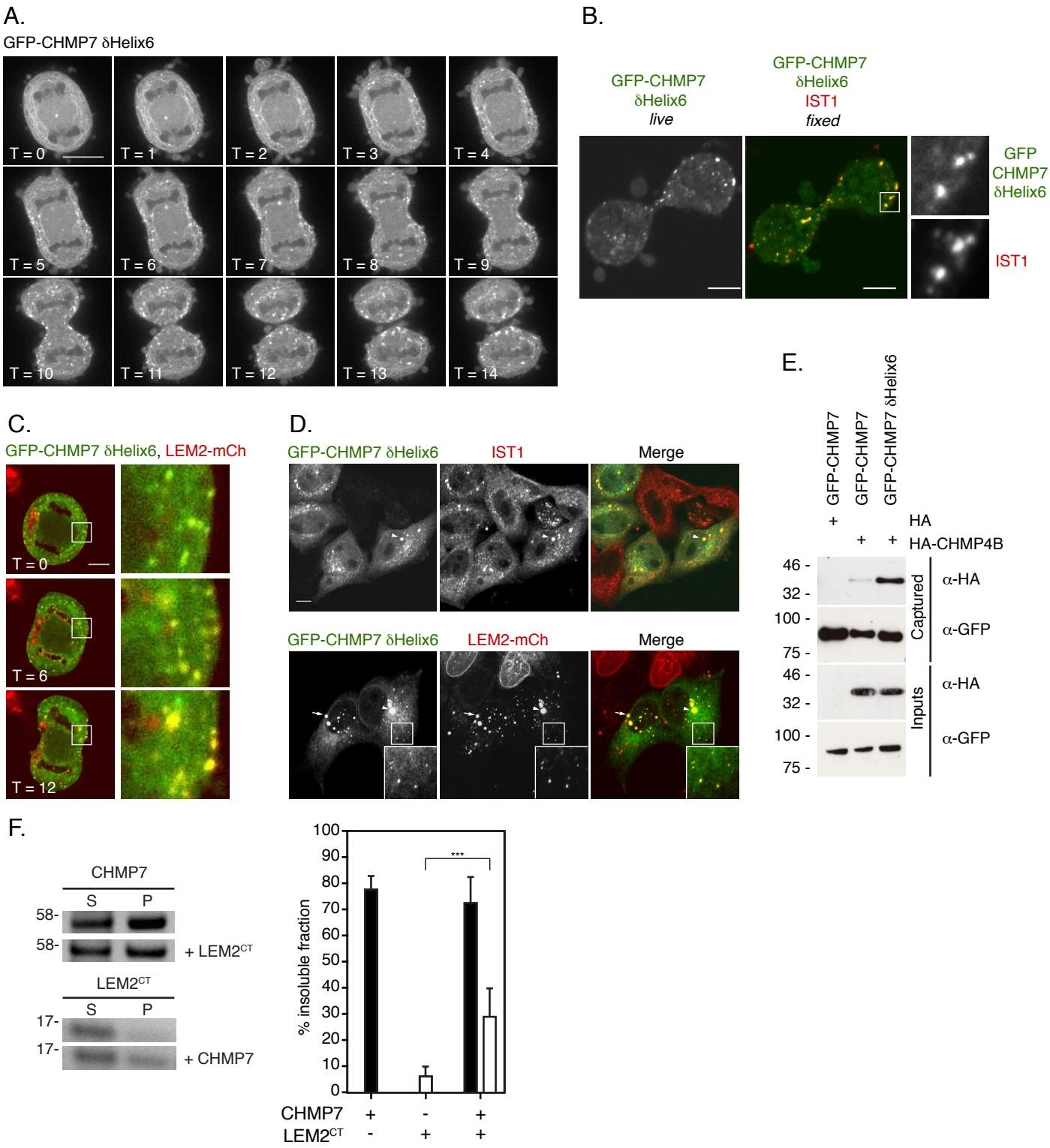

Gatta, Olmos, Stoten, Figure 3

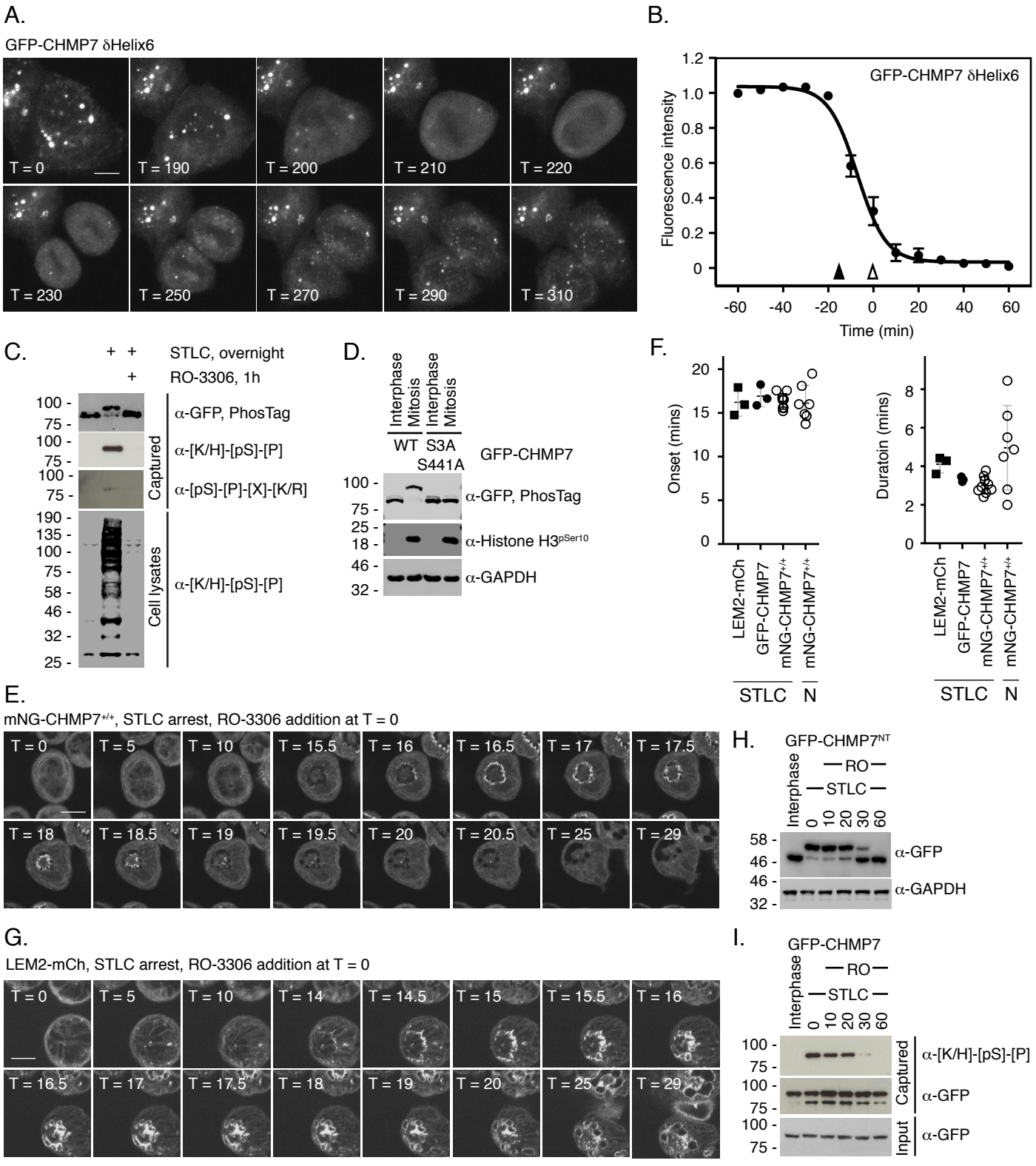

Gatta, Olmos, Stoten, Figure 4

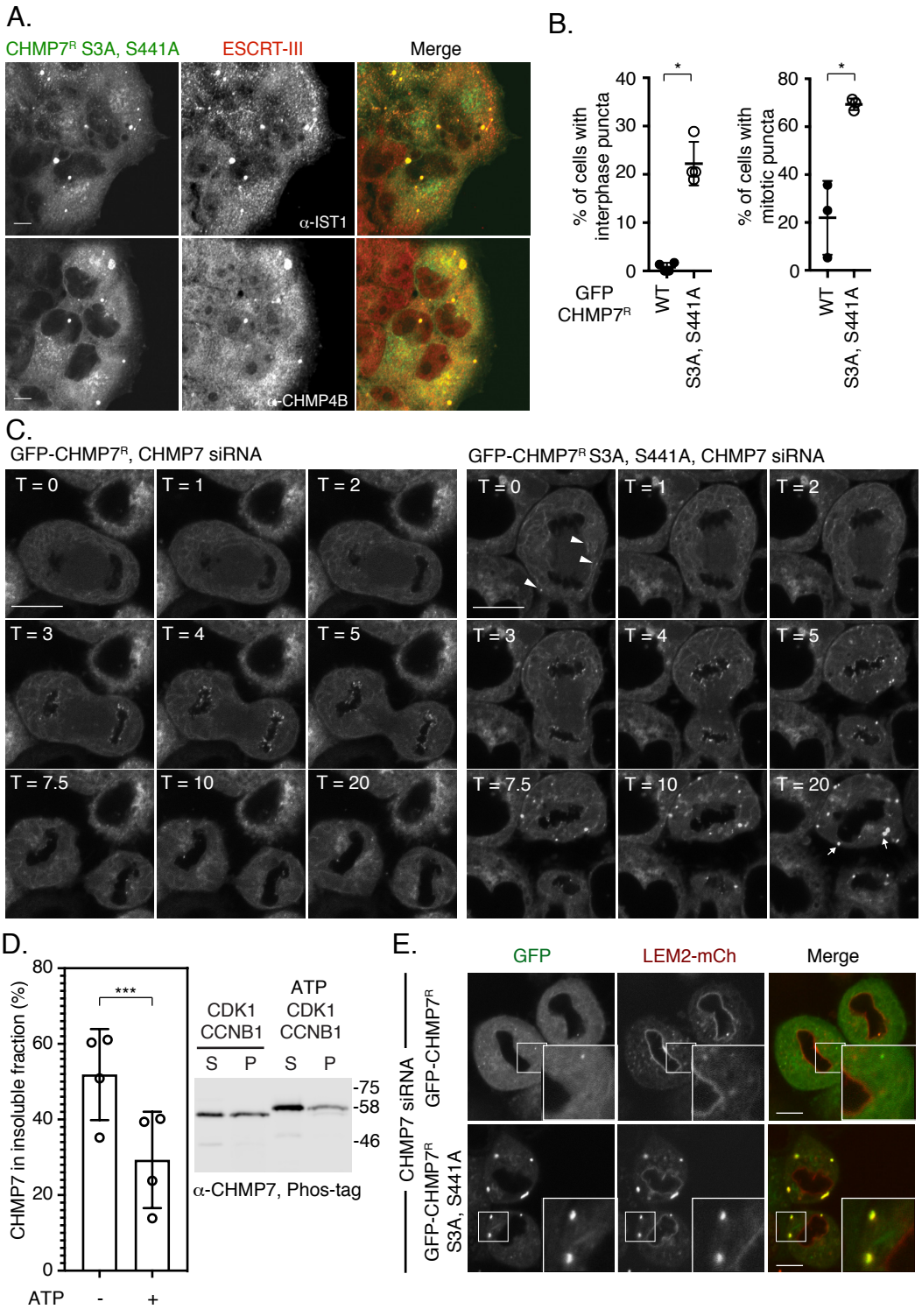

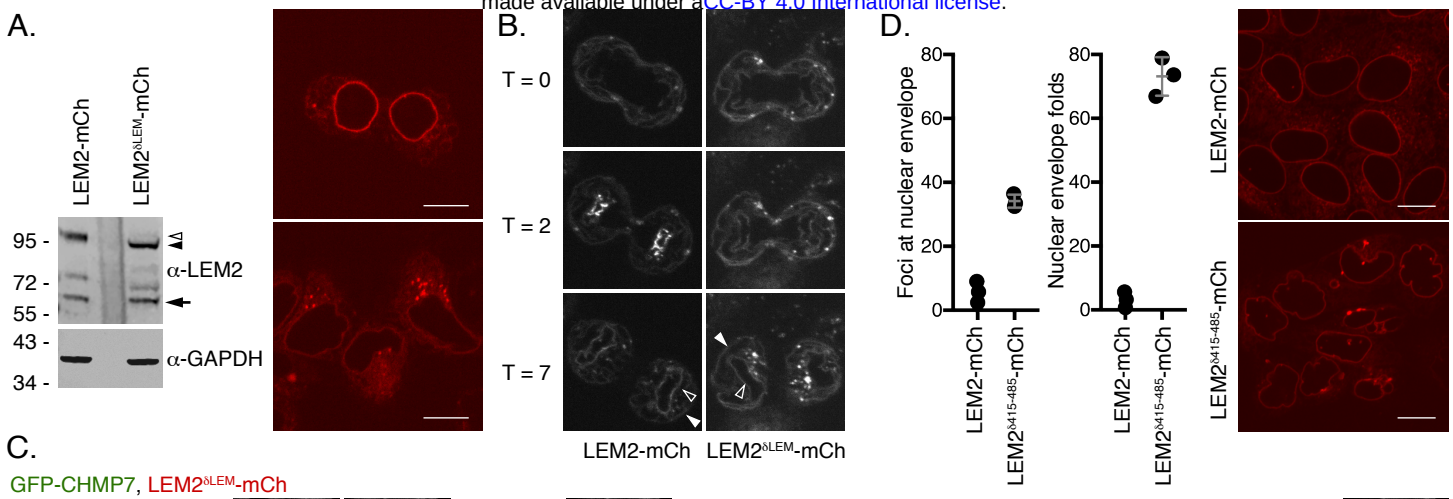

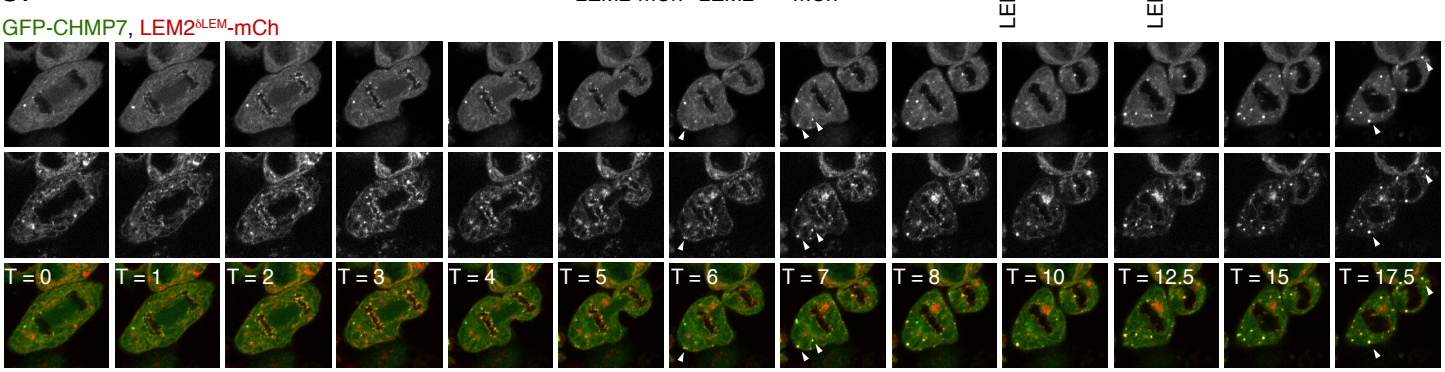

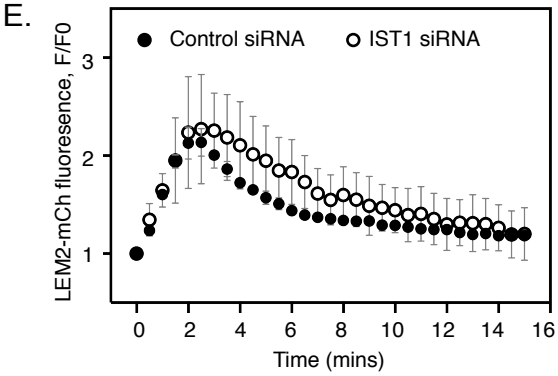

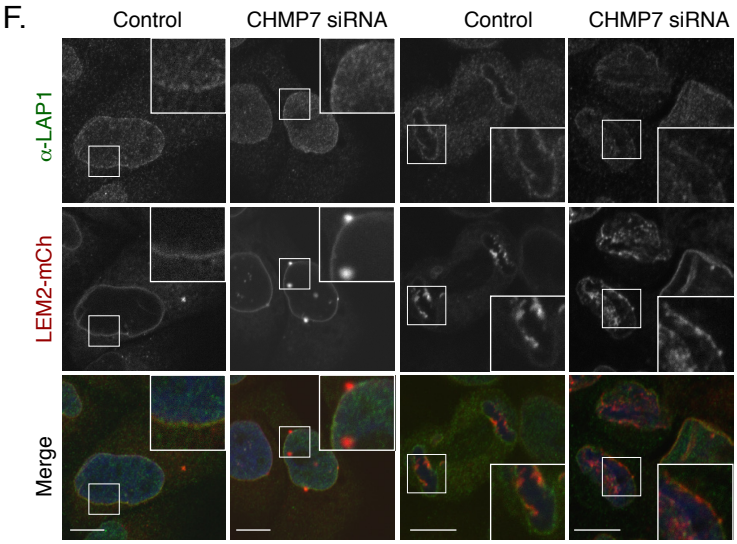

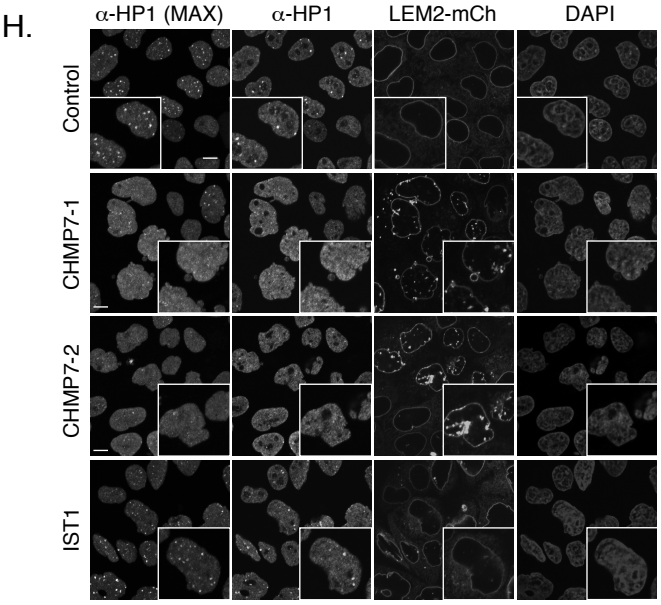

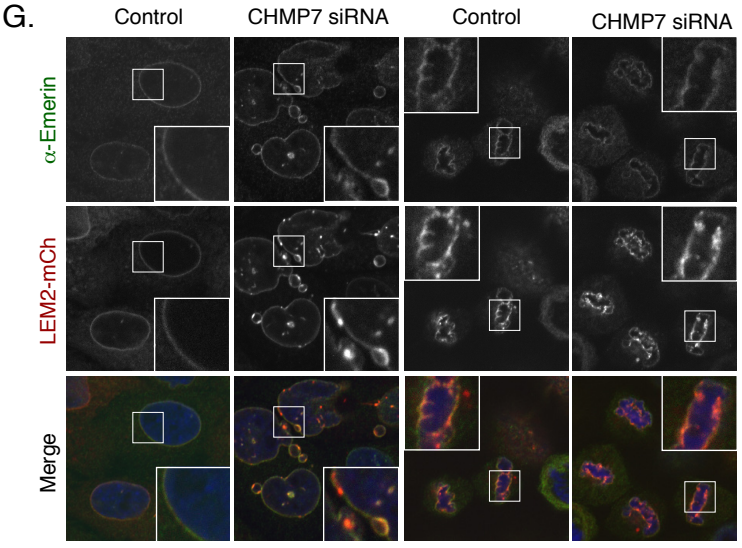

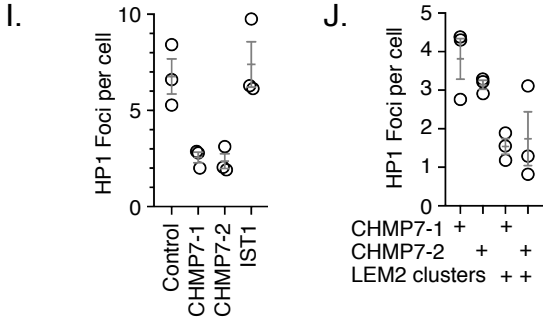

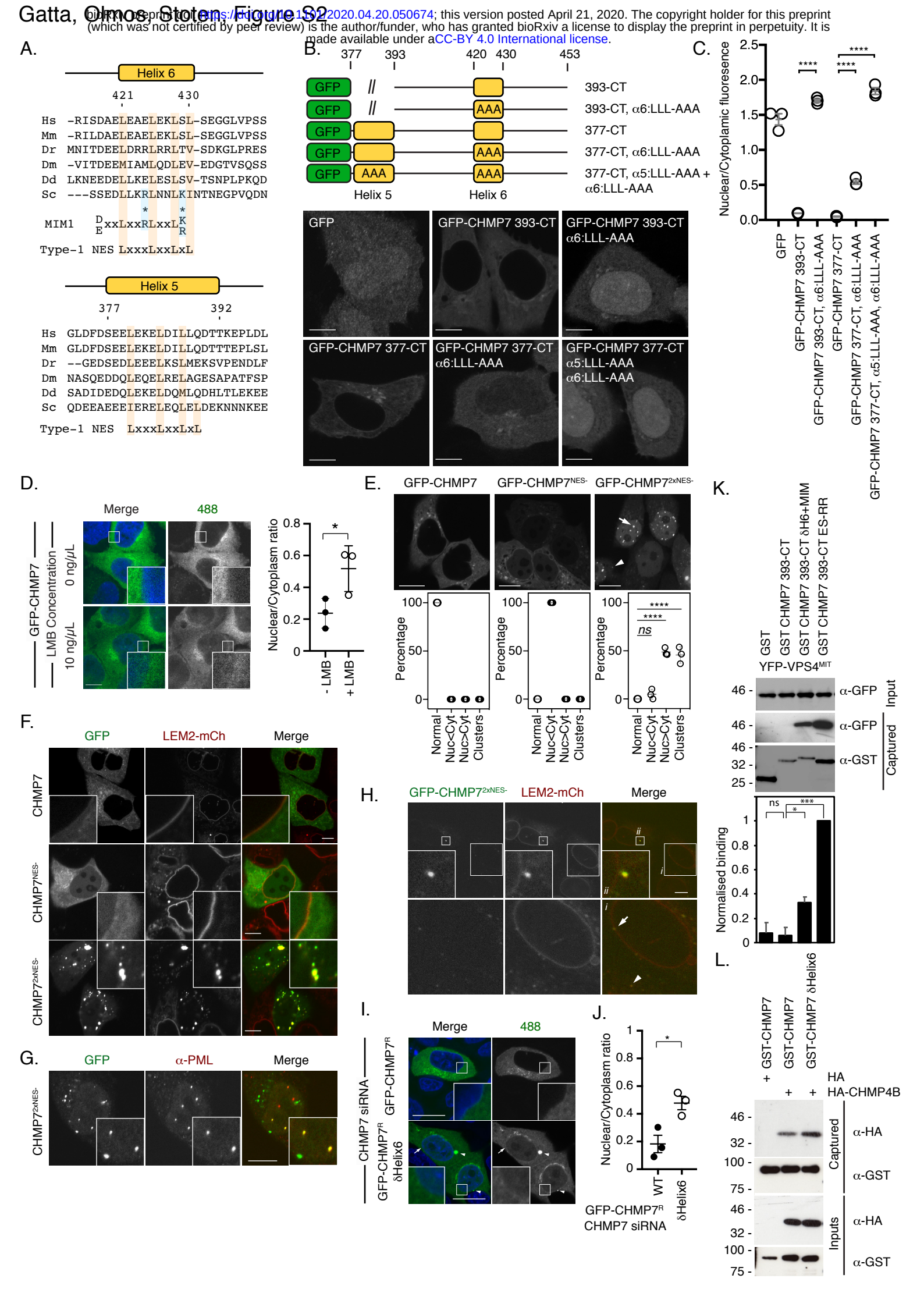

Gatta, Olmos, Stoten, Figure S3

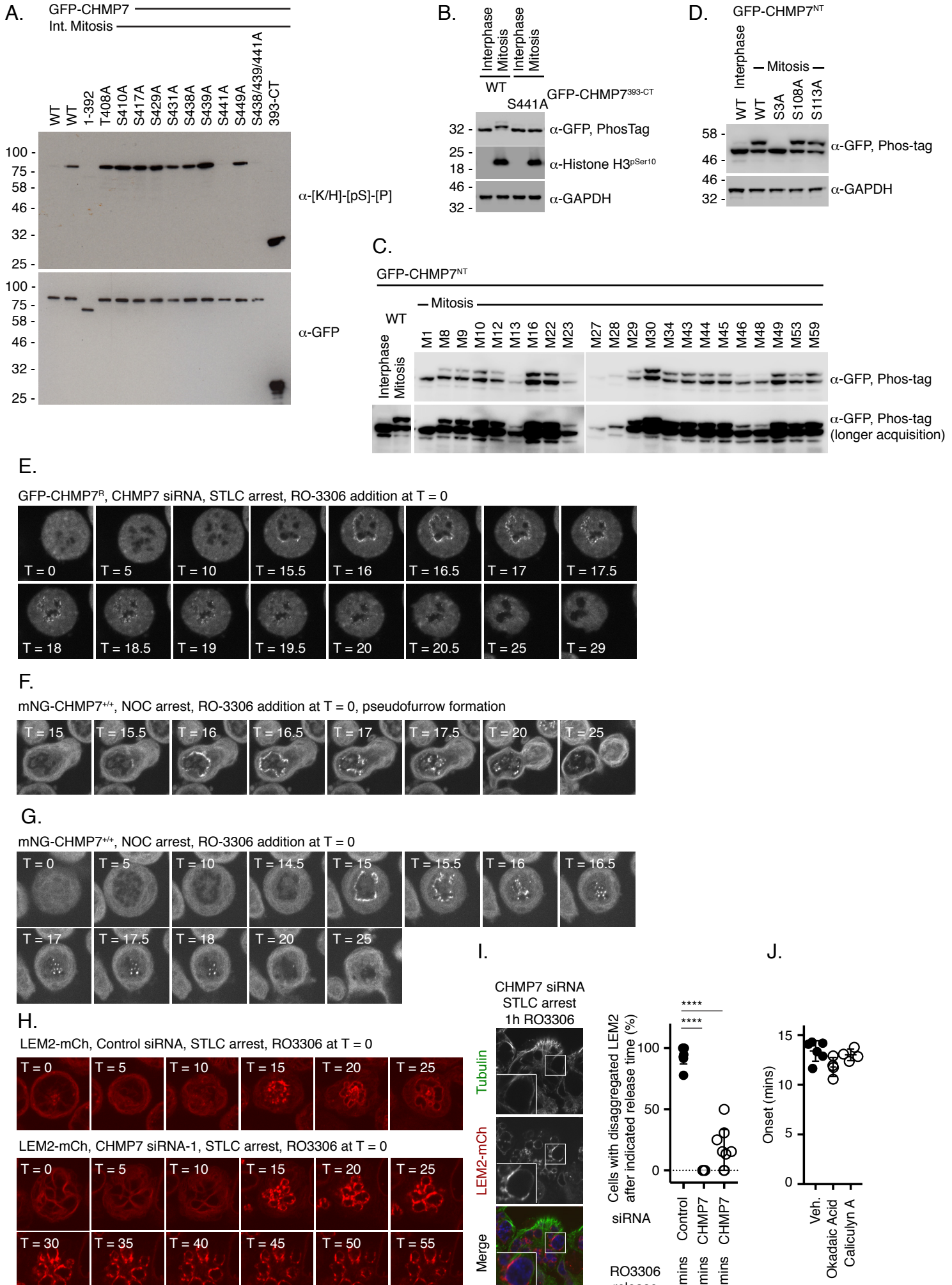

Gatta, Olmos, Stoten, Figure S4